



Enhanced spin accumulation in nano-pillar-based lateral spin valve using spin reservoir effect

Xiaomin Cui¹, Shaojie Hu^{2,3,*}  and Takashi Kimura^{2,4,*} 

¹ School of Physical Science and Technology, Northwestern Polytechnical University, Xi'an 710129, People's Republic of China

² Department of Physics, Kyushu University, 744 Motooka, Fukuoka 812-8581, Japan

³ Center for Spintronics and Quantum Systems, State Key Laboratory for Mechanical Behavior of Materials, School of Materials Science and Engineering, Xi'an Jiaotong University, Xi'an, Shaanxi, 710049, People's Republic of China

⁴ Center for Spintronics Research Network, Graduate School of Engineering Science, Osaka University, Toyonaka, Osaka 560-8531, Japan

E-mail: hu.shaojie@phys.kyushu-u.ac.jp and t-kimura@phys.kyushu-u.ac.jp

Received 17 November 2021, revised 9 December 2021

Accepted for publication 4 January 2022

Published 26 January 2022



Abstract

Lateral spin valves are ideal nanostructures for investigating spin-transport physics phenomena and promoting the development of future spintronic devices owing to dissipation-less pure spin current. The magnitude of the spin accumulation signal is well understood as a barometer for characterizing spin current devices. Here, we develop a novel fabrication method for lateral spin valves based on ferromagnetic nanopillar structures using a multi-angle deposition technique. We demonstrate that the spin-accumulation signal is effectively enhanced by reducing the lateral dimension of the nonmagnetic spin channel. The obtained results can be quantitatively explained by the confinement of the spin reservoir by considering spin diffusion into the leads. The temperature dependence of the spin accumulation signal and the influence of the thermal spin injection under a high bias current are also discussed.

Keywords: lateral spin valve, pure spin current, spin reservoir, pillar structure

(Some figures may appear in colour only in the online journal)

1. Introduction

Utilization of electron spin current rather than charge current is very important for data processing and information storage in the field of spintronics [1–4]. Especially, the pure spin current, which is a flow of angular momentum without charge current, provides an effective way for the pursuit of high-performance but low-energy-consumption electronic devices, such as magnetic sensors, spin-based nano-oscillators, hard disk readers, and spin logic devices [5–11]. The non-local lateral spin valve

(NLSV), which contains two ferromagnetic electrodes and one nonferromagnetic channel, is considered as an ideal structure for generating, manipulating and detecting pure spin current [12–14]. Lateral spin valves (LSVs) are extensively utilized to study basic physics phenomena, such as the inverse spin Hall effect, thermal spin conversion effect, anomalous Hall effect, and spin relaxation mechanisms [15–18]. To better understand the aforementioned physics phenomena and accelerate the development of related practical applications, the main appeal is to enhance the pure spin current generation, which is monitored by the spin accumulated signals.

As reported, the spin accumulated signals are remarkably improved by employing high-quality Heusler alloys, such as

* Authors to whom any correspondence should be addressed.

Co_2FeSi , $\text{Co}_2\text{Fe}(\text{Ge}_{0.5}\text{Ga}_{0.5})$ and Co_2MnSi in LSVs [19–21]. Moreover, some amorphous alloys CoFeAl and CoFeB , grown by electron-beam evaporation, can also show relatively efficient spin accumulated signals in LSVs [22, 23]. In addition, the spin accumulation signals could also be enhanced by carefully optimizing the boundary conditions and geometry structures of the spin channel [24–29]. A theoretical investigation of spin-accumulated properties has been studied by modifying the geometry of the spin reservoir in lateral spin valve structures [28]. The enhanced spin accumulation signals have been experimentally reported using a geometrical ratchet in a nonferromagnet [30]. Such an influence of the spin accumulation properties by spin injector materials, geometry structures and boundary conditions could be recognized as a spin reservoir effect. To improve the spin accumulation properties with respect to the spin reservoir effect, one of the best candidate structures is pillar-based lateral spin valves (pLSVs), where the ferromagnetic electrodes are nano-sized dots [31–34]. Compared to the wire-based lateral spin valves (wLSVs), the Joule heating effect can be significantly reduced owing to the strong heat sink in the spin channel. Therefore, a higher critical current density should be tolerated in the pLSVs. In addition, a giant pure spin current generation has been realized in pLSVs using multi-terminal injection technology [31].

So far, studies on pLSVs have been mainly based on the infinite spin transport channel, which also limits the spin reservoir effects. Moreover, grain boundary scattering and other scattering mechanisms induced by edge roughness, impurities, etc are also common performance limiters to the spin reservoir effects [35]. To overcome these limitations, we need to adopt advanced nanofabrication processing and improved structures. In this work, we successfully fabricated pLSVs with two different ferromagnetic nanodots CoFeAl and Py on a confined spin channel using a multi-angle deposition technique and dry milling process. The two different ferromagnets could help us fairly compare the spin injection efficiency of CFA by fixing the spin detector material Py . Moreover, the enhanced spin-accumulated signal was confirmed by the enhancement of spin reservoir effect.

2. Experimental results and discussion

Here, one set of devices has been fabricated on a Si substrate with a 100 nm thermal oxidation layer. First, we employ the multi-angle evaporation technique to fabricate one type of pillar-based lateral spin valve which contains CoFeAl and Py nano-dots on the confined channel. The processes of electron beam lithography and development were performed to define one Π shaped structure in the positive photoresist as shown in figure 1(a). Subsequently, a 150 nm thick Cu film was deposited at a deposition rate of 5 \AA s^{-1} at an angle normal to the substrate by Joule heat evaporation under a vacuum of $5.0 \times 10^{-6} \text{ Pa}$. Then, two closely ferromagnetic ribbons were deposited with a growing rate 0.3 \AA s^{-1} by E-beam evaporation in the same chamber at different angles,

as schematically shown in figure 1(b). The thicknesses of the CoFeAl and Py are 12 and 10 nm, respectively. It should be noted that this is a flexible way to control different ferromagnetic ribbon depositions and adjust the thickness of the layers. It's also an in-situ method to obtain high-quality ferromagnet/nonferromagnet (F/N) interface conditions without breaking the vacuum or other interface cleaning processes. Finally, a 10 nm thick Cu cap was used to prevent oxidation of the ferromagnetic layers. Another advantage is obtaining good contact with the top electrodes.

Figure 1(c) shows a scanning electron microscopy (SEM) image of the fabricated structure with bilayer ribbons. The separated distance between the two pads could be adjusted by the transversal width and deposition angle. We successfully obtained the separated stripes on the Cu pads of $1.6 \mu\text{m}$ width. The two Cu electrode legs are about 450 nm in width. Finally, we performed the nano-pillar fabrication process on the ferromagnetic ribbons by a two-steps EBL and dry ion milling processes. The pillars of the negative photoresist were fabricated by electron beam lithography, as shown in figure 1(d). After the operation of the milling process, we obtained the pillars with resist shown in figure 1(e). Then, a 68 nm SiO_2 insulator was deposited by e-beam evaporation deposition in an ultra-high vacuum. Finally, we fabricated 180 nm thick top Cu electrodes. Figure 1(f) shows a completely fabricated pillar-based LSV device with contact area sizes of $120 \text{ nm} \times 250 \text{ nm}$ and $120 \text{ nm} \times 260 \text{ nm}$ for CFA and Py , respectively. The center-to-center distance L is approximately 810 nm between the two dots for the present device. Moreover, we fabricated two additional devices with interval distances of 900 nm and 950 nm.

The spin accumulation and transport properties have been evaluated by using the standard lock-in technique with the measurement configuration shown in figure 2(a). To improve the signal-to-noise ratio, we applied a $180 \mu\text{A}$ AC current with a frequency of 173 Hz and used a lock-in amplifier to detect the output voltage. Here, the alternating current flows from one CoFeAl/Cu junction in the left to generate nonequilibrium spin accumulation. The accumulated spins diffuse in all directions away from the injector and produce spin current in the spin channel. The spin current propagates in the channel by an exponential reduction with distance from the injector. Another ferromagnetic dot could absorb part of the spin current to generate a potential difference for different magnetization directions. Thus, the generated spin current can be evaluated using the output voltage of the ferromagnet in response to various external in-plane fields in the direction of the easy axis of magnetic dots.

The typical nonlocal spin curves are shown in figure 2(b) for two different temperatures. Here, the spin signal is $0.77 \text{ m}\Omega$ at 295 K, which is defined as the normalized first-harmonic voltage difference (ΔV_S^{1f}) for the parallel and antiparallel states by the injected bias current. When the temperature is reduced to 35 K, the obtained spin signal is about $7.69 \text{ m}\Omega$, which is almost ten times larger than that at 295 K. Since the spin relaxation is dominated by the Elliott-Yafet mechanism due to the electron-phonon interaction in Cu. The

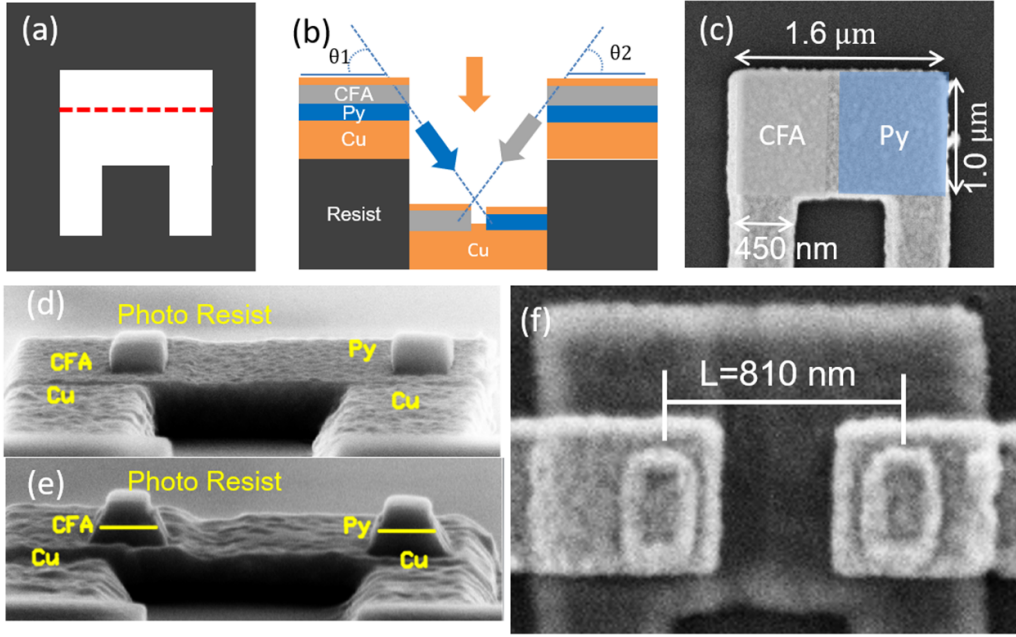


Figure 1. Illustrations of the fabrication processing for closely different ferromagnetic ribbons on the Cu buffer layer. (a) Top view of the II shape structure defined by electron beam lithography on positive photoresist. (b) Shadow evaporation illustration for ferromagnetic ribbons. First, the 150 nm thick Cu film was deposited with a deposition rate of 5 \AA s^{-1} at an angle normal to the substrate by Joule heat evaporation. Then, two closely ferromagnetic ribbons were deposited with the growing rate 0.3 \AA s^{-1} at different angles on the moderate width of Cu wire. Finally, 10 nm Cu cap layer is deposited to prevent the oxidation of ferromagnets. (c) The scanning electron microscope (SEM) image of the fabricated structure with bilayer ribbons for transversal width $1.6 \mu\text{m}$ and $1 \mu\text{m}$ length. (d) SEM of the pillars of the negative photo resist on the ribbons. (e) SEM of the pillars after the operation of the milling process. (f) SEM image of the CoFeAl/Cu/Py pillar-based lateral spin valve on the confined channel. The interval distance is about 810 nm between the two dots.

phonon scattering will be suppressed with the reduction of temperature. In addition, the increased spin diffusion length will induce such an enhancement of the spin signal at low temperatures.

In order to quantitatively evaluate the spin accumulation properties of the above devices, we borrow a one-dimensional spin diffusion model to obtain the accumulated spin signals as following [25, 28, 36]:

$$\Delta R_S = \frac{4 R_{Py} P_{Py} R_{CFA} P_{CFA} R_{Cu} e^{-L/\lambda_{Cu}}}{(R_{Py} + R_{Cu} + R_{Py} k) (R_{CFA} + R_{Cu} + R_{CFA} k) - (R_{Cu} - R_{Py} + R_{Py} k) (R_{Cu} - R_{CFA} + R_{CFA} k) e^{-2L/\lambda_{Cu}}} \quad (1)$$

where, P_{CFA} and P_{Py} are the spin polarizations for the ferromagnetic dot of CoFeAl and Py, respectively. R_{Py} , R_{CFA} and R_{Cu} represent the spin resistances for the injector, detector and Cu, respectively. The spin resistance is defined as $\rho\lambda/[S(1 - P^2)]$, where P , ρ and λ refer to the bulk spin polarization, resistivity and spin diffusion length, respectively. P is zero for a nonmagnet. S are the junction area of F/N and the crossing section area for Cu channel. λ_{Cu} is the spin diffusion length in Cu. L is the interval distance between the two ferromagnets. k is the spin resistance ratio of Cu channel and legs. If we assume the cooper's resistivity and spin diffusion length are the same for the spin channel and legs, the value of k can be replaced by the ratio of crossing section area of Cu legs and channel S_{out}/S_{ch} shown in figure 2(a). In our devices, k is evaluated as

0.36 using the cross-section area of the Cu channel and legs ($1 \mu\text{m} \times 0.110 \mu\text{m}$ and $450 \text{ nm} \times 88 \text{ nm}$).

Here, we assume that the spin diffusion length of CoFeAl and Py are $\lambda_{CoFeAl} = 2 \text{ nm}$ and $\lambda_{Py} = 2 \text{ nm}$ at 295 K. Because the electron spin relaxations in the Py, CFA, and Cu are dominated by the Elliott-Yafet mechanism, we can assume the product of spin diffusion length and resistivity is constant for them [37, 38]. The products of spin diffusion length and resistivity are $\gamma_{CFA} = \lambda_{CFA} \times \rho_{CFA} = 0.9 \text{ f}\Omega \cdot \text{m}^2$, $\gamma_{Py} = \lambda_{Py} \times \rho_{Py} = 0.71 \text{ f}\Omega \cdot \text{m}^2$ and $\gamma_{Cu} = \lambda_{Cu} \times \rho_{Cu} = 13.28 \text{ f}\Omega \cdot \text{m}^2$, respectively [23, 39]. By fitting the interval distance dependence of the spin signals in figure 2(c) using equation (1), we estimated the spin polarizations of CFA as 0.62 and 0.82 at 295 K and 35 K. For Py, the spin polarizations are 0.35 and

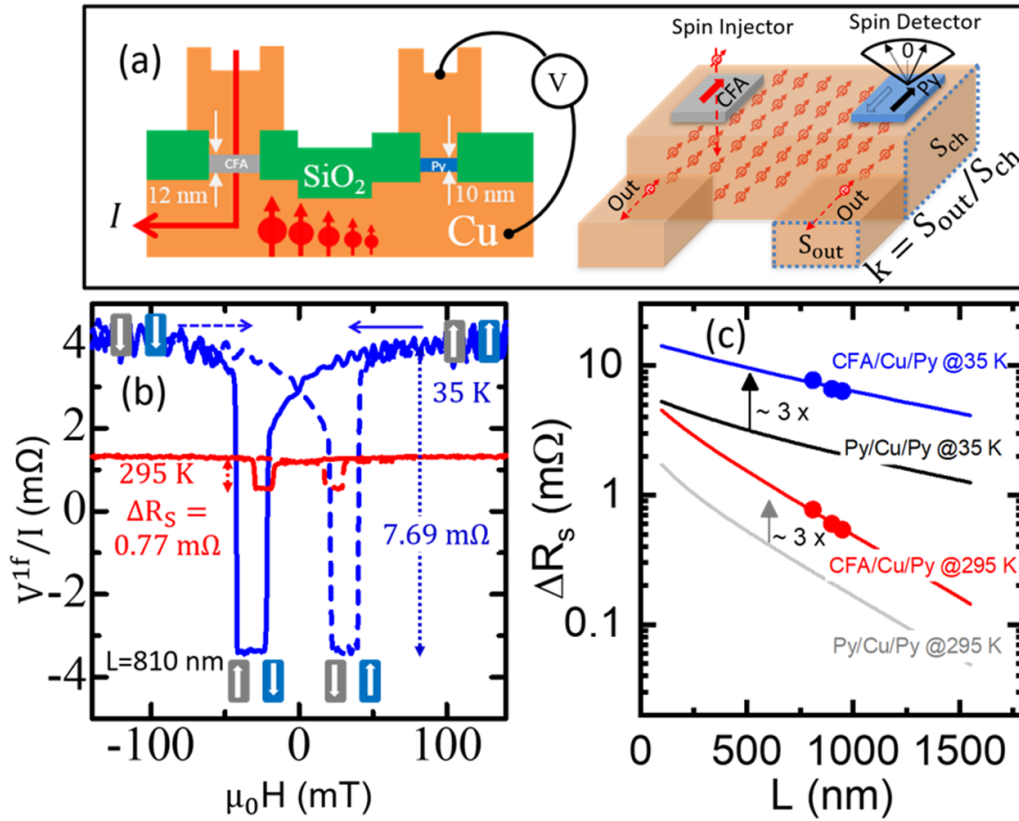


Figure 2. (a) The schematic illustration of the spin valve with the non-local spin valve measurement configuration. k is the ratio of crossing section area of Cu channel and legs S_{out}/S_{ch} . (b) Non-local spin signal curves for the lateral spin-valve device at 295 K and 35 K. The spin signal ΔR_S is defined as the overall voltage change normalized by bias current between the parallel and antiparallel states. The magnetization configurations at each state are shown by arrows. The long solid and dotted arrows indicate the direction of the field sweep. (c) Interval distance dependency of the spin signals. The blue and red solid dot symbols represent our experimental results for CFA/Cu/Py lateral spin valves at 35 K and 295 K, respectively. The blue and red lines are the fitting curves by using equation (1) for $k = 0.36$.

0.48 at 295 K and 35 K. These values are consistent with those reported previously. We also calculated the interval distance dependence of the spin signals of lateral spin valves with both Py injector and detector based on those parameters shown in figure 2(c). The numerical spin accumulated signals for the CoFeAl injector and Py detector are over a factor 3 of the Py injector and detector values at 295 and 35 K, respectively. This indicates that the spin accumulation properties are remarkably enhanced, when a high polarized material is used as the spin injector.

To further understand the spin transport properties in the confined spin channel, we also evaluated the temperature dependence of the spin signals. In order to obtain the temperature dependence of the numerical spin signal, we first show the resistivity, spin polarization, and spin diffusion length as a function of temperature. The resistivity was experimentally evaluated using 4 terminal method under an AC current of 10 μ A for CoFeAl and Py nanowires (120 nm in width, 30 nm in thickness) from 5 K to 295 K as shown in figure 3(a). As we know, the spin polarization of the ferromagnet depends on the temperature by the relation $1/(a + bT^2)$ according to Mott's two-current model [40]. We plotted the temperature dependence of spin polarization for both CoFeAl and Py in figure 3(b), based on the spin polarizations of Py and CoFeAl

at 35 and 295 K, respectively. Another important parameter is the spin diffusion length of Cu. The temperature dependence of the spin diffusion length is evaluated using the value of $\gamma_{Cu} = \lambda_{Cu} \times \rho_{Cu} = 13.28 \text{ f}\Omega \cdot \text{m}^2$ at various temperature, as shown in figure 3(c). The inset shows the experimental resistivity values of the Cu channel as a function of temperature. Based on the above results, we obtained the numerical spin-accumulated signals as a function of temperature for $k = 0.36$ and $k = 1$, as shown in figure 3(d). The spin signals of the experimental data are also plotted as a function of temperature by the solid triangles. The experimental spin signals are well fitted by equation (1) with $k = 0.36$. The spin signals are about 1.3 times larger than that of the $k = 1$. This means that for $k = 1$, the spin current will be much easier to follow out of the channel, and the spin reservoir effect will be weak, resulting in fewer spins accumulated at the detector. Due to the reduced outflow of spin current from the confined channel, such pLSVs with the confined spin channel can increase spin accumulation via the geometry-enhanced spin reservoir effect.

For intuitively comparing with the previously reported pillar-based lateral spin valve signals ($k = 1$), we plot the 3D color surface image of the numerical spin signal as a function of the interval distance and temperature for Py/Cu/Py,

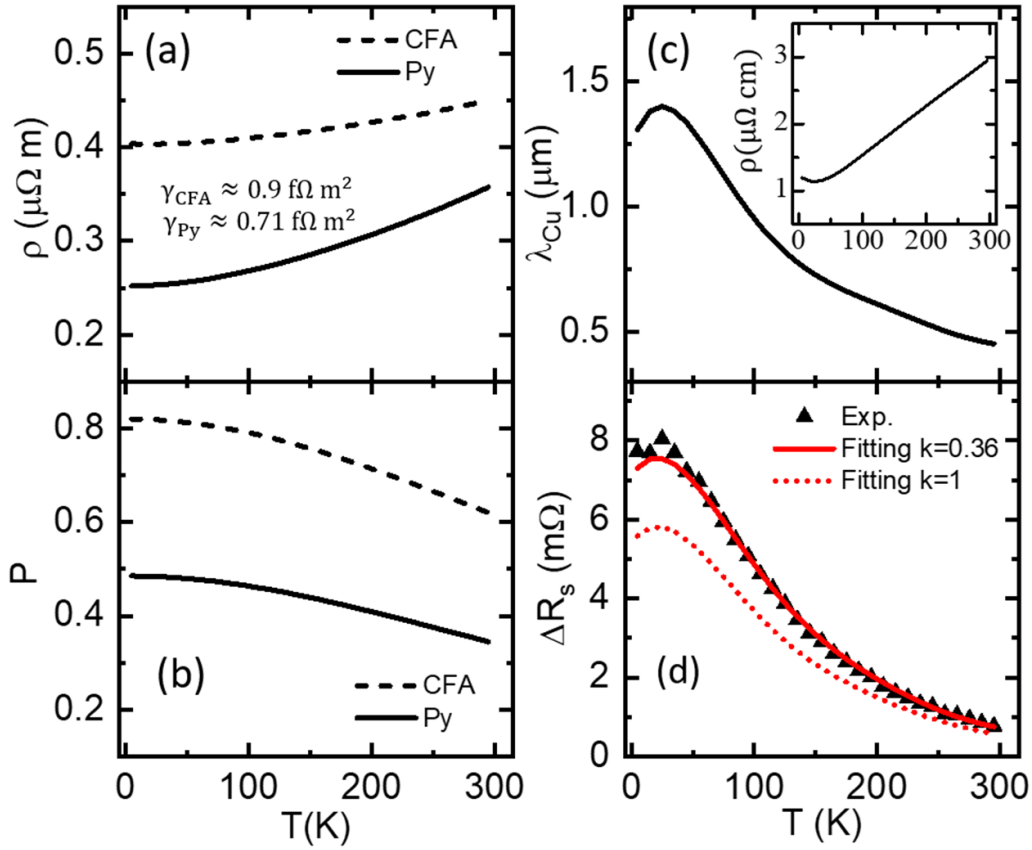


Figure 3. (a) Temperature dependence of the measured resistivity of CoFeAl and Py. The products of resistivity and spin diffusion length is defined as γ . Here, the $\gamma_{\text{CFA}} \approx 0.9 \text{ f}\Omega \cdot \text{m}^2$ and $\gamma_{\text{Py}} \approx 0.71 \text{ f}\Omega \cdot \text{m}^2$ are obtained by assuming the spin diffusion length as 2 nm at 295 K both for CoFeAl and Py, respectively. (b) Temperature dependence of the spin polarization for CoFeAl and Py. (c) Temperature dependence of spin diffusion length of Cu. The inset shows the measured temperature dependence of Cu resistivity. (d) Temperature dependence of the spin signals. The solid black triangles represent the experimental data for our present device. The numerical spin signals with the values of 0.36 and 1 are shown by the solid and dot lines, respectively.

and CFA/Cu/CFA with $k = 0.36$, as shown in figure 4. All the referenced signals are also displayed as various symbols, scaled by the same geometry size with our device [19]. Our devices' signals are almost two order higher than that of Co/Cu/Co pLSVs [34]. All the referenced experimental spin signals for Py/Cu/Py and CFA/Cu/CFA are much lower than the related numerical data. This also indicates that the geometry-induced spin reservoir effect is efficiently improved by reducing the number of spin-outflows probes in the confined channel.

Another advantage of the pLSV is the heat sink effect, which reduces or eliminates the conventional thermoelectric signals. Therefore, we systematically investigated the spin signal under the high DC bias current for understanding the influence of the Joule heating effect on such pLSVs at room temperature. Figure 5(a) shows the bias current dependence of the spin curves with the measurement configuration CFA/Cu/Py, where the CoFeAl is the injector, and Py is the detector. The spin signal is 0.81 m Ω at $I_{\text{dc}} = 0.5 \text{ mA}$, which is a bit larger than that without dc bias current. For the negative DC bias current, the spin signal shows a slight reduction. The contribution of thermal spin current had explained such modulated spin signals at CoFeAl/Cu junction under the dc bias current

[41]. And, the symmetric spin curves indicate the ANE signals vanish in such pLSVs. This is quite different from the wLSVs in our previous report [42]. Then, we also measured the spin signals under various high bias currents for the configuration of Py/Cu/CFA, where Py is the injector and CoFeAl is the detector. The base resistance still does not change significantly, even when using the $\pm 4 \text{ mA}$ bias current shown in figure 5(c). This is because thin and low-resistivity Py dot could endure much a higher bias current density. To qualitatively understand the DC bias current dependent properties, we plot the spin accumulated signals as a function of DC bias current in figure 5(c). The figure shows significant nonreciprocal features for the two measurement configurations. Because there is a significant thermal spin accumulation for CFA injection by Joule heating. However, Joule heating only induces a reduction in spin-accumulated signals for Py injection.

We also operated the second harmonic measurement to extract only the thermal spin contribution to confirm the upon scenario. Figure 6(a) shows the clear field dependence of the thermal spin curve for the configuration of CFA/Cu/Py with an AC bias current of 0.55 mA. The obtained thermal spin signal was approximately 0.07 $\Omega \cdot \text{A}^{-1}$. However, we did not observe

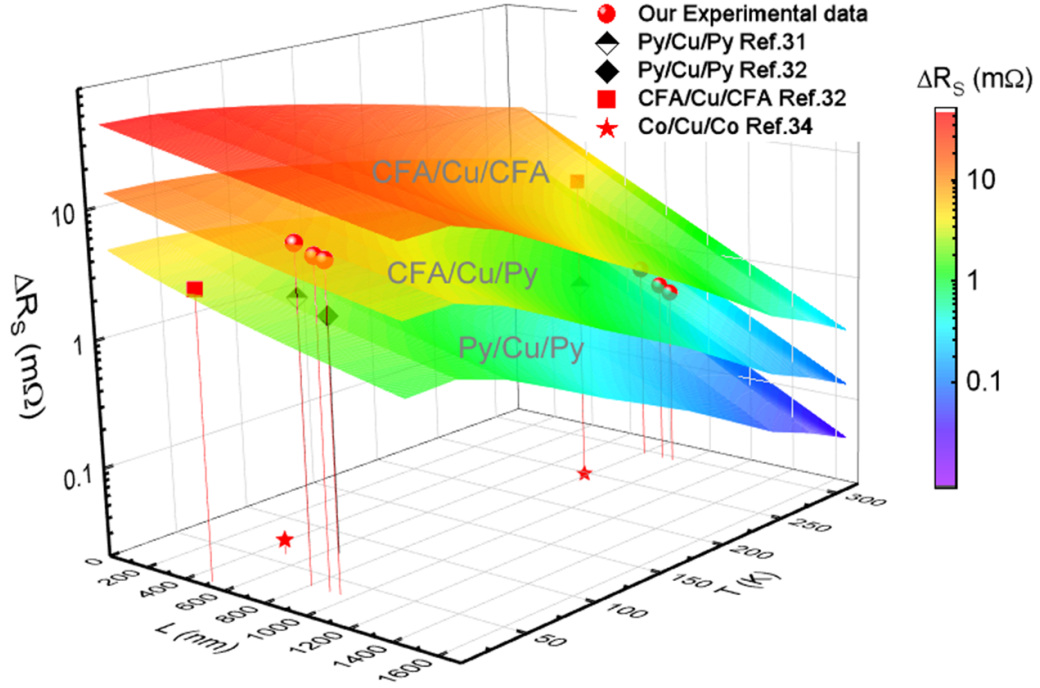


Figure 4. 3D color surface image of the spin signal as a function of interval distance and temperature calculated by equation (1) for Py/Cu/Py, CFA/Cu/CFA with $k = 0.36$. The solid red balls represent our current devices' experimental results. The previously reported pillar-based lateral spin valve signals are also displayed as various symbols, scaled by the same geometry size with our device.

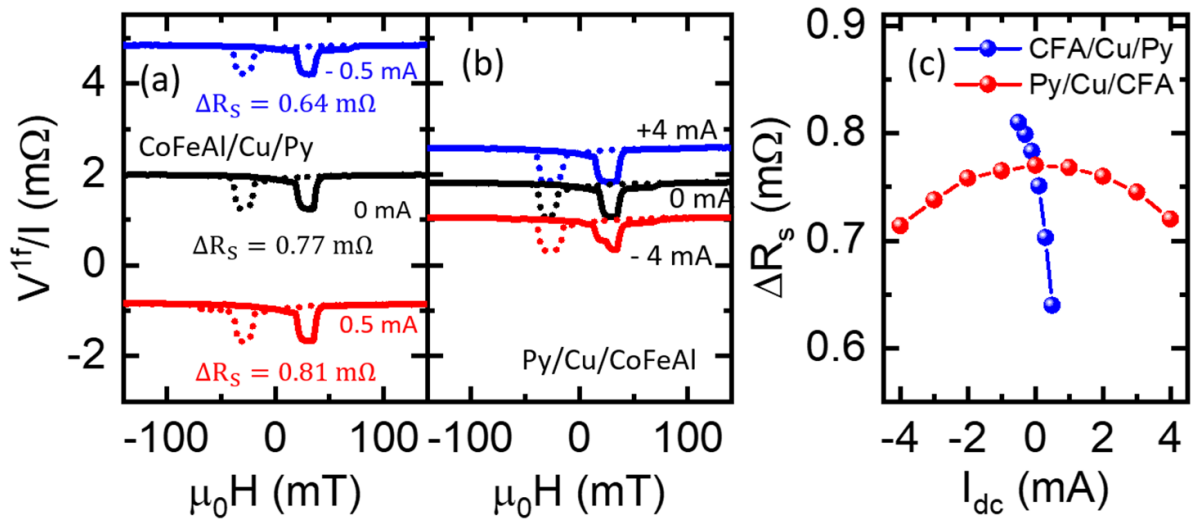


Figure 5. (a) Spin signal curves for various bias current with the measurement configuration CFA/Cu/Py (CoFeAl as injector and Py as a detector). (b) Spin signal curves for various bias current with the measurement configuration Py/Cu/CFA (Py as injector CoFeAl as a detector). (c) The spin accumulated signals as a function of DC bias current (I_{dc}) for two measurement configurations. All the bias current dependent properties are evaluated at room temperature.

a thermal spin signal in configuration of Py/Cu/CFA even an AC bias current of 4.3 mA, as shown in figure 6(b). This can be understood by considering the low spin-dependent Seebeck coefficient of Py at room temperature [39]. We can also see that the base values of the thermal spin curves are much lower for

both measurement configurations. This indicates that the thermoelectric signal is significantly suppressed in these pLSVs. Overall, the injector CFA can also enhance spin accumulation by efficient thermal spin injection under a high bias current density.

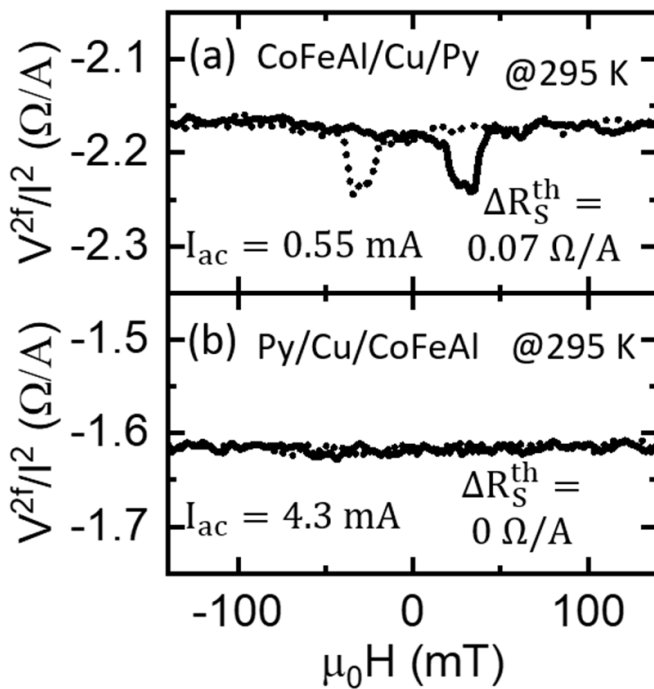


Figure 6. (a) Field dependence of the second harmonic signal curve under 0.55 mA injection current for CFA/Cu/Py measurement configuration. (b) Field dependence of the second harmonic signal curve under 4.3 mA injection current for Py/Cu/CFA measurement configuration.

3. Conclusion

In summary, we succeeded in fabricating the pillar-based lateral spin valves with the confined channel as a spin reservoir using a multi-angle deposition technique. The pLSVs consisted of two ferromagnetic dots, CoFeAl and Py with different thicknesses. We investigated the spin accumulation signals by selecting the high spin-polarization material of CoFeAl as the injector of the pLSVs. By exploiting a spin drift-diffusion model for lateral transport in ferromagnet/non-magnetic metal heterostructures, the spin accumulation signal for the CoFeAl injector was greater than a factor 3 of the value for the Py injector at 295 K and 35 K, respectively. The spin accumulation signals are enhanced by a factor of 1.3 comparing with the uniform infinite spin channel through the spin reservoir effect. Under a high bias current density, the thermoelectric effect was also strongly suppressed using such pLSVs. Moreover, the additional thermal injection of CFA enables the further enhancement of spin accumulation. Our demonstration will not only provide flexible nano-fabrication processing for designing efficient functional spin devices, but also give a new direction for further enhancing the spin signals.

Data availability statement

The data generated and/or analysed during the current study are not publicly available for legal/ethical reasons but are available from the corresponding author on reasonable request.

Acknowledgments

This work was partially supported by the National Key Research Program of China (Grant No. 2017YFA0206202), International Postdoctoral Exchange Fellowship Program (20190083), JSPS KAKENHI Grant number 17H06227, 21H05021 and, JST CREST (JPMJCR18J1). Thank you very much for the fruitful discussions with Prof. Jaroslav Hamrle from the Technical University of Ostrava of Czech Republic.

ORCID iDs

Shaojie Hu  <https://orcid.org/0000-0003-3799-972X>
Takashi Kimura  <https://orcid.org/0000-0002-1253-2130>

References

- [1] Wolf S A 2001 *Science* **294** 1488–95
- [2] Žutić I, Fabian J and Das Sarma S 2004 *Rev. Mod. Phys.* **76** 323–410
- [3] Bader S and Parkin S 2010 *Annu. Rev. Condens. Matter Phys.* **1** 71–88
- [4] Maekawa S, Valenzuela S O, Saitoh E and Kimura T 2017 *Spin Current* vol 22 (Oxford: Oxford University Press)
- [5] Demidov V E, Urazhdin S and Demokritov S O 2010 *Nat. Mater.* **9** 984–8
- [6] Demidov V E, Urazhdin S, Ulrichs H, Tiberkevich V, Slavin A, Baither D, Schmitz G and Demokritov S O 2012 *Nat. Mater.* **11** 1028–31
- [7] Chumak A V, Vasyuchka V I, Serga A A and Hillebrands B 2015 *Nat. Phys.* **11** 453–61
- [8] Dery H, Dalal P, Cywiński Ł and Sham L J 2007 *Nature* **447** 573–6
- [9] Xu Y, Xia K and Ma Z 2008 *Nanotechnology* **19** 235404
- [10] Bandyopadhyay S and Cahay M 2009 *Nanotechnology* **20** 412001
- [11] Manipatruni S, Nikonov D E and Young I A 2016 *Phys. Rev. Appl.* **5** 014002
- [12] Johnson M and Silsbee R H 1985 *Phys. Rev. Lett.* **55** 1790–3
- [13] Jedema F J, Filip a T and van Wees B J 2001 *Nature* **410** 345–8
- [14] Bakaul S R, Hu S and Kimura T 2013 *Appl. Phys. A* **111** 355–60
- [15] Kimura T, Otani Y, Sato T, Takahashi S and Maekawa S 2007 *Phys. Rev. Lett.* **98** 156601
- [16] Slachter A, Bakker F L, Adam J-P and van Wees B J 2010 *Nat. Phys.* **6** 879–82
- [17] Benítez L A, Sierra J F, Savero Torres W, Arrighi A, Bonell F, Costache M V and Valenzuela S O 2018 *Nat. Phys.* **14** 303–8
- [18] Qin C, Chen S, Cai Y, Kandaz F and Ji Y 2017 *Phys. Rev. B* **96** 134418
- [19] Kimura T, Hashimoto N, Yamada S, Miyao M and Hamaya K 2012 *NPG Asia Mater.* **4** e13
- [20] Takahashi Y K, Kasai S, Hirayama S, Mitani S and Hono K 2012 *Appl. Phys. Lett.* **100** 052405
- [21] Pfeiffer A, Hu S, Reeve R M, Kronenberg A, Jourdan M, Kimura T and Kläui M 2015 *Appl. Phys. Lett.* **107** 082401
- [22] Bridoux G, Costache M V, Van de Vondel J, Neumann I and Valenzuela S O 2011 *Appl. Phys. Lett.* **99** 102107
- [23] Hu S, Itoh H and Kimura T 2014 *NPG Asia Mater.* **6** e127
- [24] Ji Y, Hoffmann A, Jiang J S and Bader S D 2004 *Appl. Phys. Lett.* **85** 6218–20
- [25] Kimura T, Hamrle J and Otani Y 2005 *Phys. Rev. B* **72** 014461

- [26] Yang T, Kimura T and Otani Y 2008 *Nat. Phys.* **4** 851–4
- [27] Laczkowski P, Vila L, Nguyen V-D, Marty A, Attané J-P, Jaffrès H, George J-M and Fert A 2012 *Phys. Rev. B* **85** 220404
- [28] Stejskal O, Hamrle J, Pištora J and Otani Y 2016 *J. Magn. Mater.* **414** 132–43
- [29] Savero Torres W, Laczkowski P, Nguyen V D, Rojas Sanchez J C, Vila L, Marty A, Jamet M and Attané J P 2014 *Nano Lett.* **14** 4016–402
- [30] Abdullah R M, Vick A J, Murphy B A and Hirohata A 2014 *J. Phys. D: Appl. Phys.* **47** 482001
- [31] Nonoguchi S, Nomura T and Kimura T 2012 *Appl. Phys. Lett.* **100** 132401
- [32] Nomura T, Ohnishi K and Kimura T 2016 *AIP Conf. Proc.* **1763** 020011
- [33] Nomura T, Ohnishi K and Kimura T 2016 *J. Appl. Phys.* **120** 142121
- [34] Smith A K, Jamali M, Stecklein G, Crowell P A and Wang J-P 2016 *IEEE Magn. Lett.* **7** 3103604
- [35] Masourakis E, Arzubiaga L and Mihajlović G, Villamor E, Llopis R, Casanova F and Hueso L E 2016 *Nanotechnology* **27** 095201
- [36] Takahashi S and Maekawa S 2003 *Phys. Rev. B* **67** 052409
- [37] Villamor E, Isasa M, Hueso L E and Casanova F 2013 *Phys. Rev. B* **87** 094417
- [38] Sagasta E, Omori Y, Isasa M, Otani Y, Hueso L E and Casanova F 2017 *Appl. Phys. Lett.* **111** 082407
- [39] Hu S, Zhao J, Wang L, Cui X, Ohnishi K, Aiki T, Min T, Xia K and Kimura T 2018 *Phys. Rev. Mater.* **2** 104403
- [40] Mott N F 1936 *Proc. R. Soc. A* **153** 699–717
- [41] Hu S, Cui X, Nomura T, Min T and Kimura T 2017 *Phys. Rev. B* **95** 100403
- [42] Hu S and Kimura T 2013 *Phys. Rev. B* **87** 014424